Microchimica Acta (2025) 192:217
https://doi.org/10.1007/s00604-025-07070-8

RESEARCH

Synthesis of trypsin-protected $CsPbCl_3$ fluorescent nanocrystals for hydroxyl radical sensing

Suresh Kumar Kailasa[1] · Kartik Pankajbhai Makwana[1] · Madhura Pradeep Deshpande[2] · Yoojin Choi[2] · Ruth Stephanie[2] · Chan Yeong Park[2] · Tae Jung Park[2]

Received: 12 November 2024 / Accepted: 25 February 2025

Abstract

Water-dispersible perovskite nanocrystals (PNCs) show promising applications in recognizing ionic and molecular species because of their excellent optical properties. However, lead halide PNCs have some limitations when they are used as probes for molecular species sensing in aqueous media. Here, we introduce trypsin (Try) as a bioligand for the synthesis of cesium lead chloride ($CsPbCl_3$) PNCs with high water stability. The as-fabricated Try-$CsPbCl_3$ PNCs show $\lambda_{Em/Ex}$ at 433/370 nm with a quantum yield of 17.26%. The fluorescence emission spectral characteristics of Try-$CsPbCl_3$ PNCs demonstrated that water-stable Try-$CsPbCl_3$ PNCs acted as a promising fluorescent probe for the detection of hydroxyl radical ($^{\bullet}OH$) via turn-off mechanism. The Try-$CsPbCl_3$ PNCs-based turn-off fluorescence approach displayed good selectivity for hydroxyl radical in water, showing a wider linear range (0.01–5 μM) with a remarkable detection limit of 3.10 nM for hydroxyl radical. The Try-$CsPbCl_3$ PNCs were demonstrated to be a facile probe for sensing $^{\bullet}OH$ in water samples, which signifies that Try-$CsPbCl_3$ PNCs exhibited broad applications for hydroxyl radical sensing in real samples.

Keywords Try-$CsPbCl_3$ PNCs · Hydroxyl radical · Fluorescence spectrometry · HR-TEM

Introduction

In recent years, lead halide perovskite nanocrystals (PNCs) have emerged as outstanding materials in fabricating solar cells, sensors, light-emitting diodes, and optoelectronic devices because of their remarkable characteristics including superior quantum yield (QY), narrow full width at half-maximum, impressive charge transport capabilities, high photocatalytic properties, and tunable emission wavelength in complete visible and near-infrared region [1–5]. Interestingly, it was noticed that perovskite oxides are quite stable in water, whereas lead halide PNCs are highly unstable in water and easily degraded by exposing them to heat, light, and moisture [6–8], resulting in limiting their promising applications in multidisciplinary research.

To improve lead halide PNCs water stability, several researchers have introduced different strategies to fabricate lead halide PNCs including lead chloride PNCs with high water stability. For example, perflorocompounds were used as ligands for the preparation of water-stable $CsPbBr_3@Cs_4PbBr_6$ PNCs [9]. Furthermore, various polymers (poly(l-lactide) polypropylene glycol, polysulfone [10], NH_2-PEG-COOH [11], NH_2 group terminated hyperbranched polymer [12], polymethyl methacrylate [13], polystyrene [14], polystyrene-cetyltrimethylammonium bromide [15], and polyethylene glycol [16]), organic molecules (ethylenediaminetetraacetic acid [17], bolaamphiphilic ligand (NKE-12) [18], adamantane-1-amine [19], (4,4′-bipyridine and 2,2′-bipyridine) [20], glycyrrhizic acid [21], 4-bromobutyric acid-oleylamine [22], oleylamine-oleic acid [23], and oleic acid-3-bromopropionic acid [24]), and inorganic salts and compounds (cesium trifluoroacetate [25], $MAPbBr_3$@ lead laurate [26], mesoporous silica [27], Al_2O_3 [28], metal–organic frameworks [29], ZrO_2 [30], and TiO_2 [31]), respectively. The above approaches successfully produced high stability of lead halide PNCs without losing their fluorescence properties, suggesting encapsulation of lead halide PNCs with suitable ligand chemistry offers several

✉ Tae Jung Park
tjpark@cau.ac.kr

[1] Department of Chemistry, Sardar Vallabhbhai National Institute of Technology, Surat 395 007, India

[2] Department of Chemistry, Research Institute of Chem-Bio Diagnostic Technology, Chung-Ang University, 84, Heukseok-Ro, Dongjak-Gu, Seoul 06974, Republic of Korea

Published online: 10 March 2025

features such as water stability, good QY, and superior optical properties. Furthermore, it is a very challenging task to design water- and air-stable lead chloride PNCs without the use of complicated synthetic approaches as well as ligand chemistry. Since hydroxyl radical is selectively damaged, the protein structures include trypsin [32]. Furthermore, free radicals including hydroxyl radicals were effectively inactivated trypsin by the oxidation of trypsin residues to N-formylkynurenine and other residues [33]. In order to alter the surface chemistry and fluorescence properties of $CsPbCl_3$ PNCs, trypsin (Try) was explored as a bioligand for the preparation of water-stable $CsPbCl_3$ PNCs in the sensing of hydroxyl radical.

Reactive oxygen species (ROS) are produced by mitochondria in the cells, exhibiting a highly reactive nature [34]. The ROS (oxygen-containing radicals-superoxide, peroxyl, hydroxyl ($^{\bullet}OH$), and hydroperoxyl) and non-radical agents, ozone, HOCl, and H_2O_2, which are easily converted into ROS, play a key role in numerous biochemical pathways in the cells [35]. It was observed that certain levels of ROS efficiently enhance cellular functions (migration, proliferation, and differentiation) [36]. However, ROS have potentially induced oxidative stress and cell damage, which yield cell death [37]. Among ROS, hydroxyl radical is recognized as one of the highly reactive ROS, exhibiting a lifetime in the nanoseconds [38, 39]. Usually, hydroxyl radical is produced in in vivo via oxygen molecule oxidation to superoxide, higher levels of $^{\bullet}OH$ cause oxidative damage to various bio-macromolecules (nucleic acids, lipids, carbohydrates, and proteins), demonstrating that significant attention must be paid to monitoring of $^{\bullet}OH$ in cells and various environments. Importantly, $^{\bullet}OH$ plays a key role in initiating numerous free radical-induced reactions (oxidation of many organic and inorganic chemical species via electron transfer reactions and addition reactions), favoring to boost-up advanced oxidation process, which improves the removal of organic and inorganic pollutants from environmental water and wastewater treatment plants [40, 41]. It was also observed that the levels of $^{\bullet}OH$ can enhance the biotreatability of agro- and pharmaceutical and industrial wastewaters, thereby minimizing concentrations of toxic organic and inorganic species via degradation process [42, 43]. These reports illustrated that $^{\bullet}OH$ is widely present in aquatic regions, exhibiting an essential role in biochemical cycles. In order to identify $^{\bullet}OH$ radical, several analytical techniques such as electrochemical, electron spin resonance, fluorescence, and UV–visible spectroscopic and high-performance liquid chromatographic techniques have been applied to detect ROS including $^{\bullet}OH$ radical [44–52]. Importantly, several fluorescent probes including terbium complexes [38], Coumarin–Neutral Red [47], copper and molybdenum nanoclusters [53, 54], Ag–Au nanocages [55], carbon dot-based hydrogel [56], and dihydroquinolines have been utilized as fluorescence probes for sensing of $^{\bullet}OH$ radical with lower limit of detection (LOD) [57]. The nanomaterial- and organic molecule-based fluorescence probes have proven to be promising readers to selective assay of $^{\bullet}OH$ in biological and environmental systems. Due to their complex procedures in fabricating fluorescence probes, there is a still necessity to introduce a facile and novel fluorescence probe for $^{\bullet}OH$ sensing in water samples.

In this work, we report a simple and selective hydroxyl radical ($^{\bullet}OH$) sensing strategy using aqueous-stable trypsin (Try) encapsulated cesium lead chloride ($CsPbCl_3$) PNCs as a nanoprobe (Scheme 1). The as-synthesized Try-$CsPbCl_3$ PNCs were stable in aqueous medium and displayed spherical shape morphology with a mean size of 2.5 ± 0.5 nm. Further, Try-$CsPbCl_3$ PNCs exhibited blue fluorescence under UV lamp (365 nm), showing $\lambda_{Em/Ex}$ at 433/370 nm, which offers a QY of 17.26%. Noticeably, the emission intensity of Try-$CsPbCl_3$ PNCs was quenched by hydroxyl radical, leading to the development of a fluorescence turn-off approach for $^{\bullet}OH$ assay with an LOD of 3.10 nM. The developed sensing strategy was used to detect $^{\bullet}OH$ in water samples, demonstrating Try-$CsPbCl_3$ PNCs-based fluorescence method could be an effective tool for monitoring $^{\bullet}OH$ in real samples.

Experimental section

Materials and instruments

Lead (II) chloride ($PbCl_2$, 98%) and cesium chloride (CsCl, 99.99%) were produced from SRL and BLD pharm, respectively. Trypsin was obtained from Enzyme Bioscience Pvt. Ltd. (Surat, Gujarat, India) as a gift sample. 1-Octadecene (ODE) and potassium superoxide (KO_2) were obtained from Sigma-Aldrich (St. Louis, MO, USA); N-bromo succinimide (NBS), sodium hypochlorite (NaOCl), and hydrogen peroxide (H_2O_2) were purchased from SRL, FINAR, and SDFCL Chemicals, respectively. Deionized water was used for the preparation of solutions and sensing experiments, and analytical-grade chemicals were utilized without any further purification.

The as-prepared Try-$CsPbCl_3$ PNCs size and morphology were investigated using field emission transmission electron microscopy (FETEM) (JEOL-200, Tokyo, Japan). Fluorescence (emission and excitation) spectra of Try-$CsPbCl_3$ PNCs were examined by a Cary Eclipse fluorescence spectrometer (Agilent Technologies, Santa Clara, CA, USA). UV/Vis absorption spectra were recorded with a Maya Pro 2000 spectrophotometer (Ocean Optics, Orlando, FL, USA). Infrared spectra of Try-$CsPbCl_3$ PNCs were examined with an ALPHA II Fourier transform infrared (FT-IR) spectrometer (Bruker,

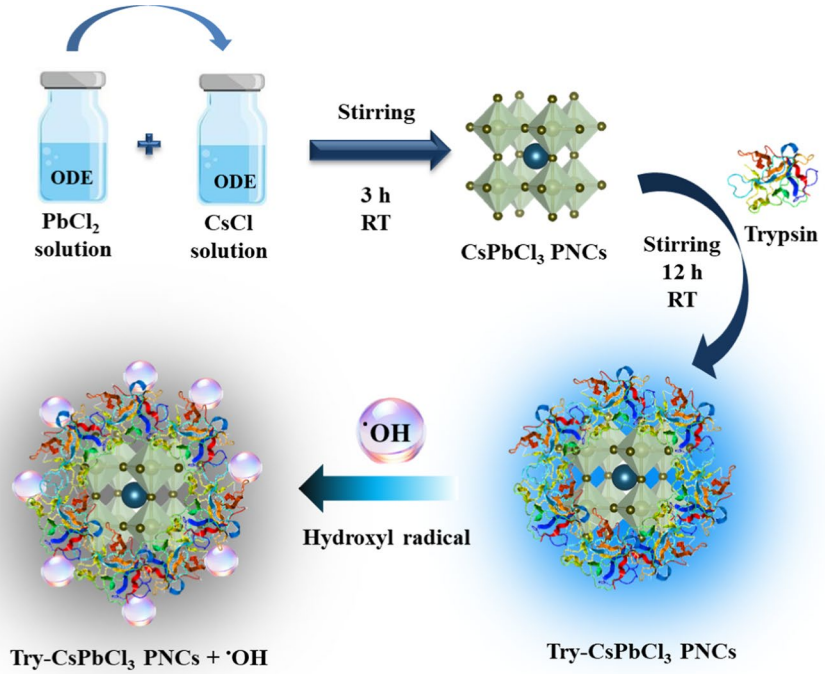

Scheme 1 Schematic illustration for Try-$CsPbCl_3$ PNCs synthesis and sensing of •OH

Billerica, MA, USA). X-ray diffraction (XRD) spectrum of Try-$CsPbCl_3$ PNCs was recorded using a D8-Advance Instrument (Bruker AXS). X-ray photoelectron spectroscopy (XPS) (K-alpha +, Thermo Fisher Scientific, Waltham, MA, USA) was performed for the confirmation of the elemental composition of Try-$CsPbCl_3$ PNCs. Hydrodynamic diameter and zeta potentials of Try-$CsPbCl_3$ PNCs were obtained using a NanoZS90 nanoparticle size potential analyzer (Malvern, UK).

Synthesis of try-$CsPbCl_3$ PNCs

Blue fluorescence water-stable $CsPbCl_3$ PNCs were prepared with a slight modification [58, 59] using Try as a ligand via a simple reaction. Firstly, 100 mM (33.6 mg) of $PbCl_2$ and 100 mM (55.6 mg) of CsCl precursors were dispersed in 2 mL of ODE separately and stirred for 30 min at room temperature. Then, the preparation of $CsPbCl_3$ PNCs was initiated by mixing both solutions in 10 mL of reaction flask. The mixture was stirred at room temperature for 3 h. The formed $CsPbCl_3$ PNCs were capped with Try by adding Try (32 mg) into $CsPbCl_3$ solution (4.0 mL) and then stirred for 12 h, triggering the formation of blue fluorescent Try-$CsPbCl_3$ PNCs. The formed Try-$CsPbCl_3$ PNCs were washed with hexane and then dispersed in water for sensing applications.

Fluorescence sensing of ·OH using try-$CsPbCl_3$ PNCs as a turn-off probe

In the sensing study, the following reactive species solutions were prepared as follows, hydroxyl radical (•OH) solution was prepared via the Fenton reaction (•OH and OH^- were produced by the reaction between Fe^{2+} and H_2O_2), superoxide anion ($^{\bullet}O_2^-$) was prepared by using 0.711 mg of KO_2 in 10 mL DMSO, and other species (MnO_4^-, $Cr_2O_7^{2-}$, HPO_4^{2-}, $S_2O_8^{2-}$, and NBS) were generated by dissolving their salts in water. For •OH sensing, the as-prepared Try-$CsPbCl_3$ PNCs were used to detect •OH radical, and the fluorescence spectra of Try-$CsPbCl_3$ PNCs (1 mL, 2.45 mg/mL) were investigated with different concentrations of •OH radical (0.5 mL). Briefly, 1.0 mM of •OH radical was generated by mixing Fe^{2+} ion (1 mM) with H_2O_2 (10%) at a volume ratio of 1:1. Different concentrations of •OH radical (0.01–500 µM, 0.5 mL) were treated separately with 1 mL of Try-$CsPbCl_3$ PNCs (2.45 mg/mL), and then their emission spectra were recorded, leading to establish good calibration graph between the ratio of I_0/I at 433 nm and concentrations of •OH radical. To ensure the selectivity of Try-$CsPbCl_3$ PNCs, different chemical species (MnO_4^-, $Cr_2O_7^{2-}$, HPO_4^{2-}, $S_2O_8^{2-}$, $O_2^{\bullet-}$, and NBS) were added separately into Try-$CsPbCl_3$ PNCs solutions and examined their impact on the emission spectral intensities of Try-$CsPbCl_3$ PNCs. The fluorescence emission spectra of Try-$CsPbCl_3$

PNCs were recorded with λ_{Ex} at 370 nm for •OH radical sensing and selectivity tests. The selectivity of Try-$CsPbCl_3$ PNCs toward •OH radical was evaluated by investigating the emission spectra of Try-$CsPbCl_3$ PNCs in the presence of various biomolecules (cysteine, arginine, tryptophan, and alanine, 500 µM), cations (Na^+, Ca^{2+}, Mg^{2+}, Zn^{2+}, Cu^{2+}, and Fe^{3+}, 500 µM), and anions (Cl^-, I^-, Br^-, PO_4^{3-}, and SO_4^{2-}, 500 µM) with and without addition of •OH radical.

Fluorescence detection of ˙OH radical in water samples

To apply potential application of the probe, tap and river waters from Tapi River, Surat, Gujarat, India, were used in the present study. The water samples were filtered through a microfilter and then treated the sample with different concentrations (0.01, 0.1, 0.5, 1.0, 2.5, 5.0, 10.0, and 25.0 µM) of •OH radical and then introduced 1 mL of Try-$CsPbCl_3$ PNCs and vortexed for 2 min. The fluorescence emission intensities of Try-$CsPbCl_3$ PNCs at 433 nm were examined, and the spectral studies were repeated three times and represented the statistical data as mean ± relative standard deviation (RSD).

Results and discussion

Synthesis and characterization of Try-$CsPbCl_3$ PNCs

The synthesis pathway for the preparation of Try-$CsPbCl_3$ PNCs and their application for •OH radical sensing in aqueous medium were shown in Scheme 1. Initially, the influence of Try concentration (2–10 mg/mL) was studied on the fluorescence spectra of $CsPbCl_3$ PNCs using $PbCl_2$ (100 mM) and CsCl (100 mM) as precursors (Figure S1). Upon increasing Try concentration from 2.0 to 8.0 mg/mL, the intensity of fluorescence emission spectra of $CsPbCl_3$ PNCs was increased; however, the emission intensity was decreased by using 10 mg/mL of Try due to the excessive Try molecules on Try functionalized $CsPbCl_3$ PNCs, which leads to form Try-$CsPbCl_3$ PNCs nanoaggregates that will result to quench the emission peak of $CsPbCl_3$ PNCs. These results suggest that 8.0 mg/mL of Try effectively enveloped $CsPbCl_3$ PNCs, thereby improving their dispersion ability in water with good fluorescence intensity. Similarly, we also investigated the optimum reaction time for the preparation of Try-$CsPbCl_3$ PNCs (Figure S2). It was clearly observed that the emission intensity of Try-$CsPbCl_3$ PNCs at 433 nm was increased with increasing reaction time from 3 to 12 h; after that, the emission peak intensity was decreased, confirming the 12 h was found to optimum reaction time for the fabrication of Try-$CsPbCl_3$ PNCs. In order to confirm the origin of emission spectra, absorption and emission spectra of Try and Try-$CsPbCl_3$ PNCs were examined and shown in Figure S3. The spectral results demonstrated that Try did not show any emission peak; however, Try-encapsulated $CsPbCl_3$ PNCs displayed a characteristic emission peak at 433 nm (Figure S3a). Interestingly, pure Try and Try-$CsPbCl_3$ PNCs exhibited different absorption spectral characteristics (Figure S3b), indicating the formation of Try-$CsPbCl_3$ PNCs. In order to investigate the role of halide ion in improving fluorescence properties and stability of Try-$CsPbX_3$ PNCs, we studied the water dispersion abilities and fluorescence properties of Try-$CsPbBr_3$ and Try-$CsPbI_3$ PNCs (Figure S4). It can be noticed that the aqueous solution of Try-$CsPbBr_3$ and Try-$CsPbI_3$ PNCs exhibited λ_{Em} at 521 and 580 nm when excited at 440 and 482 nm, respectively. It can be noticed that the emission spectra of both Try-$CsPbBr_3$ and Try-$CsPbI_3$ PNCs were blue shifted to 482, 498, 410, and 433 nm with a noticeable decrease in their intensities when the emission spectra measured after PNCs synthesis at different time intervals 3 h and 6 h. Furthermore, the emission spectra of three synthesized PNCs, i.e., Try-$CsPbCl_3$, Try-$CsPbBr_3$, and Try-$CsPbI_3$ PNCs were investigated by applying the same excitation wavelength (λ_{ex} = 370 nm) at three different times (10 min, 3 and 6 h) (Figure S5). The as-prepared Try-$CsPbCl_3$ PNCs exhibited intense emission peak spectra at three-time intervals, whereas Try-$CsPbBr_3$ PNCs showed a weak emission peak at 521 nm at 10 min as compared to Try-$CsPbCl_3$ PNCs. Noticeably, the emission spectra of Try-$CsPbBr_3$ PNCs were noticed with very weak intensity at 3 and 6 h time intervals, whereas Try-$CsPbI_3$ PNCs did not show any noticeable emission intensities at three-time intervals by applying excitation wavelength of 370 nm. These spectral results confirmed that the synthesized Try-$CsPbCl_3$ PNCs exhibited good water resistance with high emission intensity by applying λ_{ex} at 370 nm. Importantly, Try-$CsPbCl_3$ PNCs showed remarkable stability in the aqueous medium even after 6 days (Figure S3 and S6), indicating that the aqueous stability of Try-$CsPbCl_3$ PNCs is high as compared to Try-$CsPbBr_3$ and Try-$CsPbI_3$ PNCs, which promotes to use Try-$CsPbCl_3$ PNCs as a fluorescent probe.

After optimizing the reaction conditions, we examined the spectral characteristics, size, morphology, zeta potential, and elemental composition of Try-$CsPbCl_3$ PNCs. The as-fabricated Try-$CsPbCl_3$ PNCs displayed λ_{max} at 377 nm, whereas the emission/excitation peaks exhibited at 433/370 nm (Fig. 1). The obtained spectral characteristics of Try-$CsPbCl_3$ PNCs were well matched with the reported method for $CsPbCl_3$ PNCs dispersed in organic solvent (hexane) [60]. To further investigate the role of Try to encapsulate $CsPbCl_3$ PNCs, we studied the absorption and emission spectra of Try-capped $CsPbCl_3$ PNCs, unmodified $CsPbCl_3$ PNCs (dispersed in toluene and water), and pure Try (Figure S3 and S7). It can be noticed that Try capped

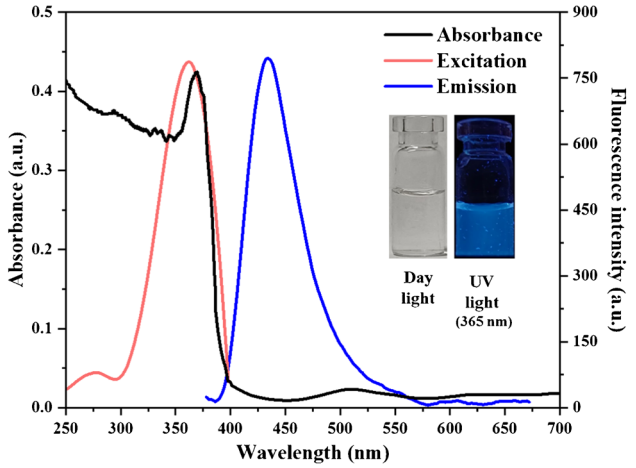

Fig. 1 Absorption (λ_{max} = 377 nm), fluorescence excitation, and emission (λ_{Ex} = 370 nm; λ_{Em} = 433 nm) spectra of Try-$CsPbCl_3$ PNCs (Inset: Digital images of Try-$CsPbCl_3$ PNCs in daylight and under UV light at 365 nm)

$CsPbCl_3$ PNCs (water), pure Try (water), and unmodified $CsPbCl_3$ PNCs (toluene) exhibited λ_{max} at 377, 301, and 355 nm, respectively, confirming that they have different absorbance values. Importantly, the characteristic emission peak of unmodified $CsPbCl_3$ PNCs exhibited good intensity when they dispersed in toluene; however, the emission spectrum of unmodified $CsPbCl_3$ PNCs does not appear when they dispersed in water, revealing that unmodified $CsPbCl_3$ PNCs exhibited poor water stability. These absorption and emission spectral data demonstrated that the water stability of $CsPbCl_3$ PNCs was greatly improved by the encapsulation of $CsPbCl_3$ PNCs with Try. Upon irradiation of Try-$CsPbCl_3$ PNCs solution with 365 nm of UV light, blue fluorescence was noticed, which confirms the formation of Try-$CsPbCl_3$ PNCs (Inset of Fig. 1). Furthermore, excitation-dependent emission spectral characteristics of Try-$CsPbCl_3$ PNCs were studied and shown in Figure S8. The emission spectral profiles of the as-prepared Try-$CsPbCl_3$ PNCs at different excitation wavelengths (300–400 nm) displayed the almost nonvariant nature in the emission spectra; however, the emission peak intensity was increased with increasing λ_{Ex} from 300 to 370 nm; after that, the intensity was decreased. The maximum emission intensity was noticed at λ_{Em} = 433 nm upon excitation of Try-$CsPbCl_3$ PNCs at λ_{Ex} = 370 nm. In addition, the fluorescence QY of Try-$CsPbCl_3$ PNCs was 17.26%, and the lifetime of Try-$CsPbCl_3$ PNCs was τ = 1.64 ns (Figure S9). In order to apply Try-$CsPbCl_3$ PNCs as a promising fluorescence probe, it is essential to investigate the stability of Try-$CsPbCl_3$ PNCs. The stability of fabricated Try-$CsPbCl_3$ PNCs in water was examined by monitoring the emission spectral profiles at different time intervals (Figure S6). The emission spectral profiles of Try-$CsPbCl_3$ PNCs exhibited almost negligible changes up to 8 days; after that, the emission peak intensity was decreased, which confirms that Try-$CsPbCl_3$ PNCs displayed good stability to use as a fluorescence probe for sensing applications.

The FT-IR spectral profiles of pure Try and Try-$CsPbCl_3$ PNCs were studied, and the data were depicted in Figure S10. The FT-IR spectrum of Try displayed a strong broad band in the range of 3600–3000 cm^{-1}, which confirms to O–H and -N–H bonds stretching vibrations. The bands at 1650 and 1523 cm^{-1} are ascribed to the amide I and II bands of Try, respectively. Similarly, the stretching vibrations of COO^-, C-N stretching, and N–H bending were noticed at 1438, 1253, and 1519 cm^{-1}, respectively. The characteristic FT-IR spectral profiles of Try were completely changed due to the encapsulation of $CsPbCl_3$ PNCs. It can be observed that a noticeable decrease in the intensity of broadband in the range of 3600–3000 cm^{-1} for -OH and $-NH_2$ groups stretching and a drastic shift in the characteristic amide bands confirm the backbone structural deformation in Try due to the formation of Try encapsulated $CsPbCl_3$ PNCs. Size and morphological analyses of the as-synthesized Try-$CsPbCl_3$ PNCs were further confirmed by using FE-TEM and dynamic light scattering (DLS) (Fig. 2 and Figure S11a). The as-prepared Try-$CsPbCl_3$ PNCs are nearly spherical shape with a mean size of 2.5 ± 0.5 nm, suggesting that Try-$CsPbCl_3$ PNCs are highly monodispersity, as confirmed from histogram (Fig. 2a–c). The hydrodynamic diameter of Try-$CsPbCl_3$ PNCs was 10.34 nm, displaying a higher size as compared to FETEM data due to the measurement of Try-$CsPbCl_3$ PNCs with water molecules. The as-fabricated Try-$CsPbCl_3$ PNCs exhibited a negative charge (− 19.51 mV) (Figure S12a), which was confirmed by measuring zeta potential.

The elemental spectral profile of Try-$CsPbCl_3$ PNCs was further investigated by XPS, and the XPS survey spectrum of Try-$CsPbCl_3$ PNCs was shown in Fig. 3a, indicating the as-synthesized Try-$CsPbCl_3$ PNCs contains C, O, Cs, Pb, and Cl elements. Figure 3b shows the Cs 3d high resolution (HR) spectrum, displaying two peaks at 726.7 eV and 740.7 eV are correspond to the Cs $3d_{5/2}$ and Cs $3d_{3/2}$, respectively, confirming the presence of Cs^+ ion in Try-$CsPbCl_3$ PNCs. It can be observed that HR-XPS spectrum of Pb 4f exhibited two peaks at 144.7 and 139.6 eV, which are ascribed to the Pb $4f_{5/2}$ and Pb $4f_{7/2}$ of Try-$CsPbCl_3$ PNCs, respectively (Fig. 3c). Similarly, the HR spectrum of Cl 2p displayed two peaks at 200.3 and 201.8 eV, indexing to the Cl $2p_{3/2}$ and Cl $2p_{1/2}$ binding energy levels, respectively (Fig. 3d). Furthermore, the XRD pattern of Try-$CsPbCl_3$ PNCs is shown in Figure S13, exhibiting the diffraction peaks at 2θ = 15.9, 22.4, 32.2, 35.7, 43.12, 46.3, and 54.5 correspond to 100, 110, 200, 211, 220, 310, and 222 lattice planes of Try-$CsPbCl_3$ PNCs, which is well agreed with the XRD pattern of $CsPbCl_3$ PNCs [61, 62]. The as-fabricated

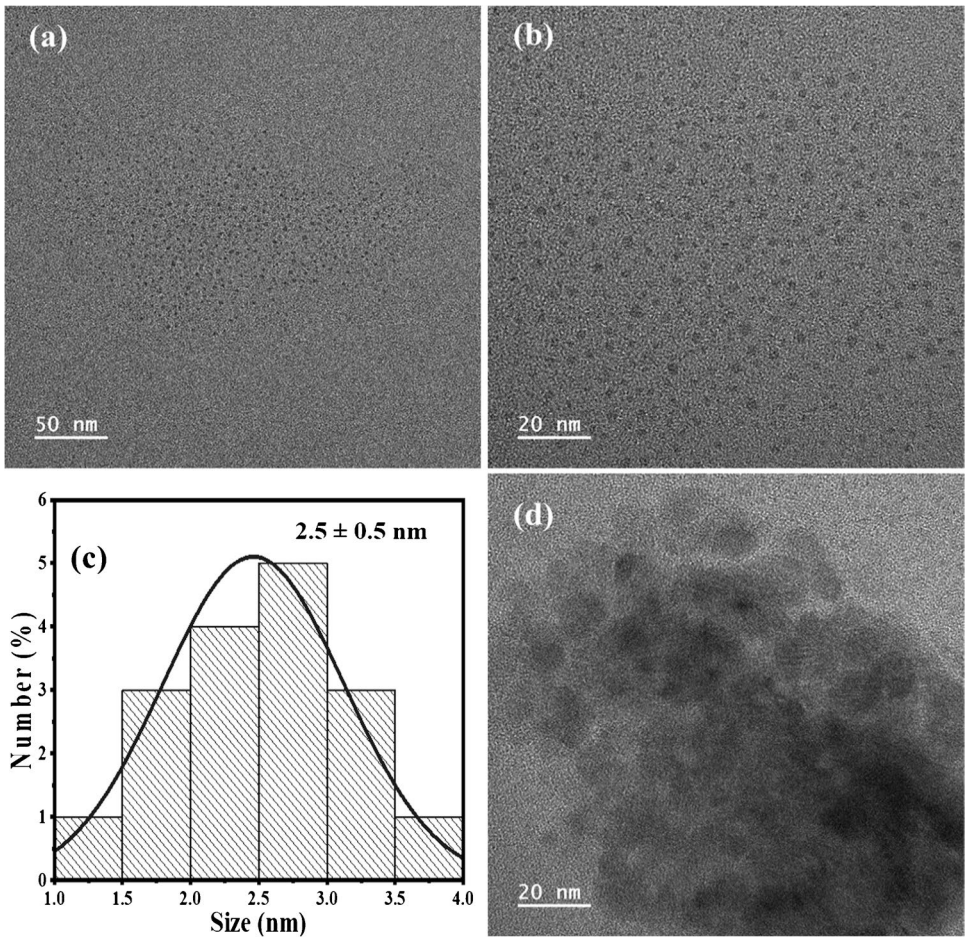

Fig. 2 HR-TEM pictures of Try-$CsPbCl_3$ PNCs with scale bars of **a** 50 nm and **b** 20 nm. **c** The size distribution of Try-$CsPbCl_3$ PNCs. **d** HR-TEM picture of Try-$CsPbCl_3$ PNCs with $^{\bullet}OH$

Try-$CsPbCl_3$ PNCs are in crystalline nature with high monodispersity. All the above data strongly support the formation of Try-$CsPbCl_3$ PNCs with monodispersity and good spectral characteristics, which explore them as potential probes for $^{\bullet}OH$ sensing.

Fluorescence sensing of $^{\bullet}OH$ radical

To examine the fluorescence detection capability of Try-$CsPbCl_3$ PNCs toward $^{\bullet}OH$ radical, several oxidizing and ROS (MnO_4^-, $Cr_2O_7^{2-}$, HPO_4^{2-}, $^{\bullet}OH$, $S_2O_8^{2-}$, $O_2^{\bullet-}$, and NBS, 1 mM, 0.5 mL) were mixed with 1 mL of Try-$CsPbCl_3$ PNCs, separately, followed by vertexing the samples for a few minutes. The fluorescence emission spectra of the samples were evaluated (Fig. 4). As can be seen, the emission spectra of Try-$CsPbCl_3$ PNCs in a significant decrease in the fluorescence emission intensity of Try-$CsPbCl_3$ PNCs was noticed in the presence of $^{\bullet}OH$ radical, while no significant fluorescence quenching was noticed in the presence of other oxidizing and ROS. These emission spectral profiles demonstrated that the as-prepared Try-$CsPbCl_3$ PNCs could be utilized as a probe for fluorescence analysis of $^{\bullet}OH$ radical in aqueous media. Moreover, the fluorescence color of Try-$CsPbCl_3$ PNCs solution with the addition of the above species was monitored under 365 nm of UV light, indicating the blue fluorescence of Try-$CsPbCl_3$ PNCs was almost non-fluorescent nature (Inset of Fig. 4), which signifies that Try-$CsPbCl_3$ PNCs act as a turn-off fluorescent probe for $^{\bullet}OH$ radical sensing. The fluorescence emission signals of Try-$CsPbCl_3$ PNCs were evaluated in the presence of phosphate-buffered saline (PBS) with pH from 2.0 to 12.0 with and without $^{\bullet}OH$ radical (Figure S14a), demonstrating that the addition of PBS pH (2.0–12.0) into Try-$CsPbCl_3$ PNCs did not affect the fluorescence spectra of Try-$CsPbCl_3$ PNCs. However, the maximum fluorescence emission quenching was observed with $^{\bullet}OH$ radical at PBS of pHs 10 and 12 (Figure S14b), and PBS of pH 10 was selected as an optimum pH for sensing of $^{\bullet}OH$ radical using Try-$CsPbCl_3$ PNCs as a probe.

Fluorescence sensing mechanism

In order to evaluate the fluorescence sensing mechanism of $^{\bullet}OH$ radical using Try-$CsPbCl_3$ PNCs as a probe, several analytical techniques (TEM, DLS, zeta potential, and lifetime) were examined. As can be seen in the FETEM image

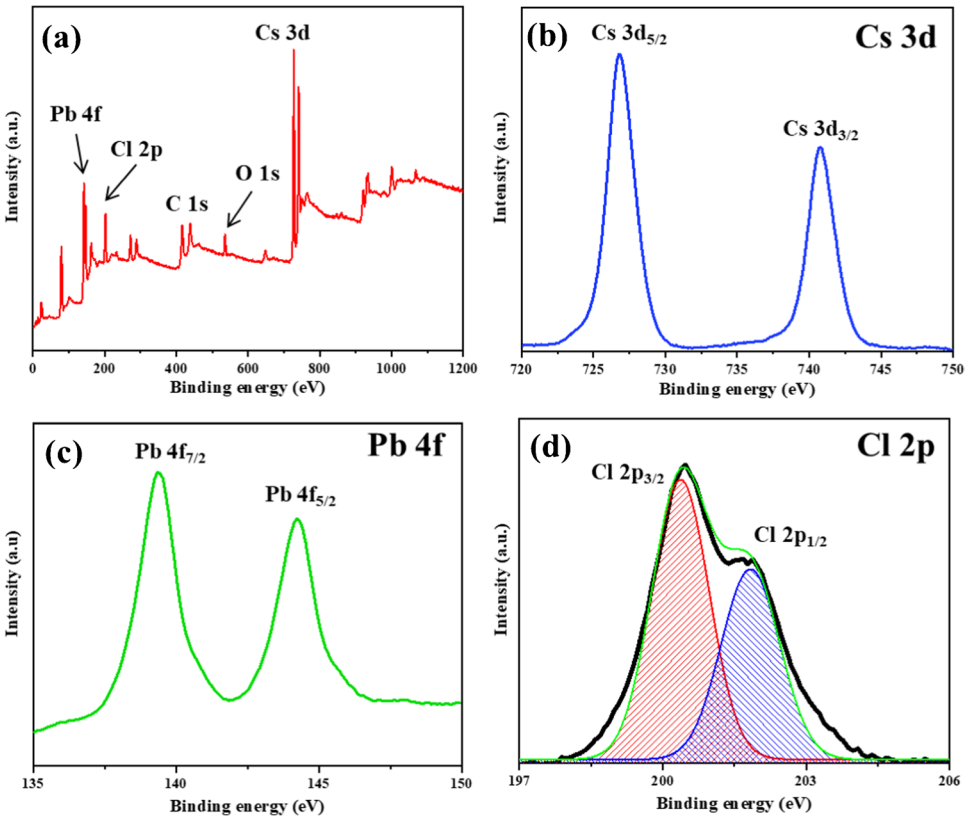

Fig. 3 XPS characterizations of Try-$CsPbCl_3$ PNCs: **a** survey spectrum, HR spectra of **b** Cs 3d, **c** Pb 4f, and **d** Cl 2p

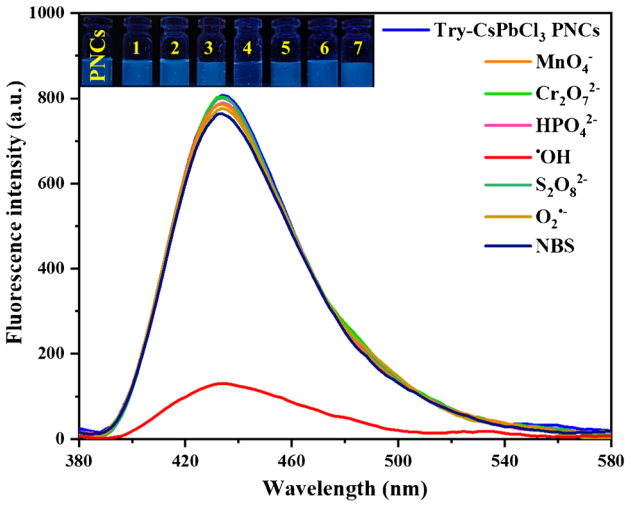

Fig. 4 Fluorescence emission spectra of Try-$CsPbCl_3$ PNCs after adding different ROS (MnO_4^-, $Cr_2O_7^{2-}$, HPO_4^{2-}, •OH, $S_2O_8^{2-}$, $O_2^{\bullet-}$, and NBS). Inset picture of Try-$CsPbCl_3$ PNCs after the addition of various ROS (1. MnO_4^-, 2. $Cr_2O_7^{2-}$, 3. HPO_4^{2-}, 4. •OH, 5. $S_2O_8^{2-}$, 6. $O_2^{\bullet-}$, and 7. NBS) under UV light (365 nm)

of Try-$CsPbCl_3$ PNCs with the addition of •OH radical (Fig. 2d), the morphology and size of Try-$CsPbCl_3$ PNCs were drastically changed by the addition of •OH radical, indicating the deformation of Try-$CsPbCl_3$ PNCs by •OH radical, which leads to form Try-$CsPbCl_3$ nanoaggregates. Similarly, the hydrodynamic diameter of Try-$CsPbCl_3$ PNCs was significantly increased to 21.5 nm by introducing •OH radical (Figure S11b), leading to destabilization of Try-$CsPbCl_3$ PNCs, which resulted in quenching the fluorescence of Try-$CsPbCl_3$ PNCs. The zeta potential of Try-$CsPbCl_3$ PNCs was − 19.51 mV; however, it was increased to − 28.23 mV (Figure S12b). Interestingly, the negligible change (from 1.64 to 1.51 ns) in the lifetime of Try-$CsPbCl_3$ PNCs was observed with the addition of •OH radical, indicating the static quenching mechanism (Figure S9). The characteristic FT-IR spectral profiles of Try-$CsPbCl_3$ PNCs were significantly changed upon the addition of •OH radical (Figure S15), suggesting the structural changes in the Try-$CsPbCl_3$ PNCs by •OH radical. Importantly, FT-IR spectral data are commonly used to examine the variations in the secondary structure of proteins and protein-chemical species interactions [32, 33]. As shown in Figure S15, the amide I and II spectral characteristics of Try were observed in the range of 1600–1700 and of 1500–1600 cm^{-1}, respectively. By comparing FT-IR spectrum of pure Try to that of Try-$CsPbCl_3$ PNCs with •OH radical, the peak intensity and peak position of the amide I (1600–1700 cm^{-1}) and II (1500–1600 cm^{-1}) bands were changed, revealing the drastic changes in the secondary structure of Try upon the addition of •OH radical. To further evaluate the inner filter effect (IFE), the fluorescence (excitation and emission) spectra of Try-$CsPbCl_3$ PNCs and the absorption spectrum of •OH

radical were studied (Figure S16), revealing the overlapping of absorption spectrum of •OH radical with excitation spectrum of Try-$CsPbCl_3$ PNCs, which confirms the IFE. Thus, the as-prepared Try-$CsPbCl_3$ PNCs act as a turn-off fluorescence probe for the detection of •OH radical.

Sensitivity

Under the optimal conditions, the variations in the fluorescence intensity of Try-$CsPbCl_3$ PNCs were investigated by adding different concentrations of •OH radical (0.01–500 µM). As can be noticed in Fig. 5, the fluorescence emission intensity of Try-$CsPbCl_3$ PNCs centered at 433 nm was gradually quenched along with increasing concentration of •OH radical. Then, the emission intensity of Try-$CsPbCl_3$ PNCs was quenched at 77% when •OH radical at 500 µM. Figure S17 displayed the constructed plot of the ratio I_0/I (where I_0 and I represent the emission intensity of Try-$CsPbCl_3$ PNCs in the absence and presence of •OH radical, respectively) against •OH radical concentration (0.01–500 µM). Furthermore, with •OH radical concentration in the range of 0.01–5.0 µM, the fluorescence quenching efficiency showed the linear fitting equation of $y = 0.2596x + 1.2061$ ($R^2 = 0.9795$) (Inset of Figure S17). The LOD was 3.10 nM (3σ/s, where "s" is the slope of the calibration curve and "σ" is the standard deviation of the blank) for •OH radical. The analytical characteristics of the developed Try-$CsPbCl_3$ PNCs-based fluorescence approach were compared with other reported methods [53, 63–70] for •OH radical sensing (Table S1), revealing the developed probe exhibited superior and comparable analytical performance with other analytical techniques for •OH radical sensing. Furthermore, the developed Try-$CsPbCl_3$ PNCs-based turn-off fluorescence strategy exhibits several analytical features such as free surface modification, simple chemical routes, good selectivity and sensitivity, and good stability in aqueous phase, which allows for use as a promising fluorescence probe for •OH radical sensing.

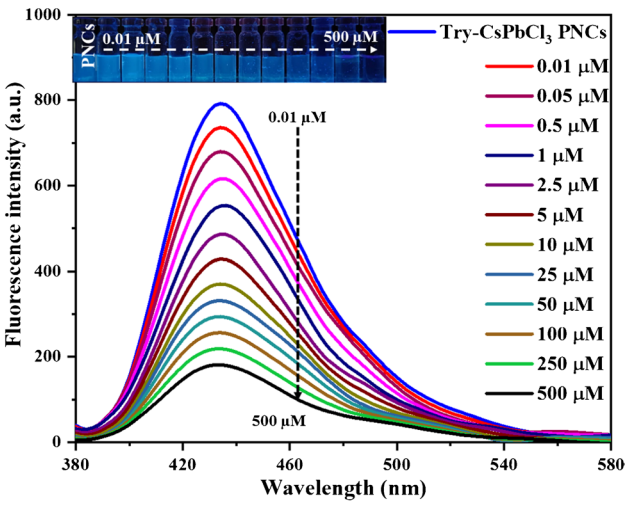

Fig. 5 Fluorescence spectra of Try-$CsPbCl_3$ PNCs in the existence of various concentrations of •OH (0.01–500 µM). Inset picture demonstrates the variations in the blue fluorescence of Try-$CsPbCl_3$ PNCs with the addition of •OH (0.01–500 µM) under UV light at 365 nm

Selectivity

The sensing selectivity of Try-$CsPbCl_3$ PNCs toward •OH radical was investigated in the presence of various metal ions, ROS, and biomolecules phosphate buffer (20 mM, pH 7.4). As shown in Figure S18, the fluorescence behavior of Try-$CsPbCl_3$ PNCs in the presence of biomolecules (cysteine, arginine, tryptophan, and alanine, 500 µM), cations (Na^+, Ca^{2+}, Mg^{2+}, Zn^{2+}, Cu^{2+}, and Fe^{3+}, 500 µM) and anions (Cl^-, I^-, Br^-, PO_4^{3-}, and SO_4^{2-}, 500 µM) is almost same and did not show any significant changes. As anticipated, Try-$CsPbCl_3$ PNCs exhibited a remarkable fluorescence quenching only with •OH radical even in the existence of the other interfering chemical species, revealing that the as-prepared Try-$CsPbCl_3$ PNCs stand out as a highly selective turn-off fluorescence probe for •OH radical sensing.

Analysis of •OH radical in water samples

To evaluate the practical application of Try-$CsPbCl_3$ PNCs in monitoring •OH radical in real samples, the collected water (tap and river) samples were filtered and subsequently added different concentrations of •OH radical (0.01, 0.1, 0.5, 1.0, 2.5, 5.0, 10.0, and 25.0 µM). Then, •OH radical treated water samples were added into Try-$CsPbCl_3$ PNCs, and their concentrations were estimated by the aforesaid procedure. From Table S2, it can be noticed that the recovery rates of •OH radical in water samples were 98.80–101.40% with a relative standard deviation of < 2.0%. In order to estimate the accuracy and precision of the developed method for the analysis of •OH radical in spiked water samples, inter- and intra-day accuracy and precision of Try-$CsPbCl_3$ PNCs-based fluorescence turn-off approach was performed, and the data were depicted in Table S3. The data showed that the percentage recoveries were in the ranges of 98.80–99.76% and 98.57–99.64% for tap and river waters. Moreover, inter- and intra-day accuracy and precision of the method are in the ranges of 0.38–1.20% and 0.5 and 1.13% for tap water and 0.42–1.29% and 0.41–0.76% for river water, respectively. The data in Table S2-S3 represent that the Try-$CsPbCl_3$ PNCs-based fluorescence method is a facile, more precision and accurate analytical approach for the detection of •OH radical in real samples, demonstrating that Try-$CsPbCl_3$ PNCs could be used as the potential fluorescence turn-off probe for the detection of •OH radical in real samples. Although the developed Try-$CsPbCl_3$ PNCs-based

fluorescence method showed good selectivity and sensitivity towards •OH radical sensing in real samples, however the synthesis of Try-$CsPbCl_3$ PNCs requires lead salts, which is a toxic nature. Furthermore, the developed method had a limitation to detect •OH radical in living cells. Overall, the as-prepared Try-$CsPbCl_3$ PNCs have good water stability for the development of a facile fluorescent probe for sensing •OH radicals in water samples with high selectivity.

Conclusions

In summary, a simple analytical tool was developed for sensing •OH radicals using water-dispersible Try-$CsPbCl_3$ PNCs as a turn-off fluorescence probe. The as-fabricated Try-$CsPbCl_3$ PNCs exhibited blue fluorescence under UV irradiation ($\lambda \sim 365$ nm) and displayed $\lambda_{Em/Ex} = 433/370$ nm. The developed Try-$CsPbCl_3$ PNCs-based fluorescence approach has a highly selective and sensitive response toward •OH radical with a good linearity in the concentration range of 0.01–5.0 µM, which achieves the LOD of 3.10 nM. Importantly, Try-$CsPbCl_3$ PNCs exhibit superior selectivity for •OH radical with virtually no fluorescence quenching by other interfering chemical species (ROS, metal ions, anions, and biomolecules). Furthermore, Try-$CsPbCl_3$ PNCs-based analytical approach was successfully applied to detect •OH radical in water samples. Thus, the as-synthesized Try-$CsPbCl_3$ PNCs could be successfully integrated with fluorescence spectrometry for the detection of •OH radical in real samples.

Supplementary Information The online version contains supplementary material available at https://doi.org/10.1007/s00604-025-07070-8.

Acknowledgements SKK thanks the Director, Sardar Vallabhbhai National Institute of Technology, Surat for granting the sabbatical leave for Brainpool Programme at Chung-Ang University, South Korea. This research was supported by the Chung-Ang University Basic Science Research Grants in 2025.

Author contribution Suresh Kumar Kailasa: Methodology, Formal analysis, Writing—original draft. Kartik Pankajbhai Makwana: Material preparation, Formal analysis, Writing—Review and Editing. Madhura Pradeep Deshpande: Formal analysis, Data collection and analysis, Writing—Review and Editing. Yoojin Choi: Formal analysis, Data collection and analysis, Writing—Review and Editing. Ruth Stephanie: Data collection and analysis, Writing—Review and Editing. Chan Yeong Park: Formal analysis, Writing—Review and Editing. Tae Jung Park: Conception and design, Data collection and analysis, Formal analysis and Investigation, Software, Funding, Writing—review & editing. All authors reviewed the manuscript.

Funding Open Access funding enabled and organized by Chung-Ang University. This research was supported by the Brain Pool program funded by the Ministry of Science and ICT through the National Research Foundation of Korea (RS-2023–00221526).

Data availability Data will be available from corresponding author on demand.

Declarations

Ethical approval Not applicable.

Consent to participate Not applicable.

Consent for publication Not applicable.

Conflict of interest The authors declare no competing interests.

References

1. Chen J-K, Zhao Q, Shirahata N, Yin J, Bakr OM, Mohammed OF, Sun H-T (2021) Shining light on the structure of lead halide perovskite nanocrystals. ACS Mater Lett 3:845–861
2. Peighambardoust NS, Sadeghi E, Aydemir U (2022) Lead halide perovskite quantum dots for photovoltaics and photocatalysis: a review. ACS Appl Nano Mater 5:14092–14132
3. Kang W, Niu Y, Lu M, Wei Y, Li H, Xie X (2023) Inorganic lead halide perovskite micro-/nanostructures: from self-assembly to applications. ACS Appl Electron Mater 5:2956–2969
4. Patel MR, Singh PDD, Harshita, Basu H, Choi Y, Murthy ZVP, Park TJ, Kailasa SK (2024) Single crystal perovskites: synthetic strategies, properties and applications in sensing, detectors, solar cells and energy storage devices. Coord Chem Rev 519:216105
5. Kailasa SK, Vajubhai GN, Koduru JR, Park TJ, Hussain CM (2021) Recent progress on the modifications of ultra-small perovskite nanomaterials for sensing applications. Trends Anal Chem 144:116432
6. Vajubhai GN, Chetti P, Kailasa SK (2022) Perovskite quantum dots for fluorescence turn-off detection of the clodinafop pesticide in food samples via liquid–liquid microextraction. ACS Appl Nano Mater 5:18220–18228
7. Chan KK, Huajun DG, Sum HTC, Yong K-T (2021) Water-stable all-inorganic perovskite nanocrystals with nonlinear optical properties for targeted multiphoton bioimaging. ACS Appl Nano Mater 4:9022–9033
8. Huang S, Wang B, Zhang Q, Li Z, Shan A, Li L (2018) Post-synthesis potassium-modification method to improve stability of $CsPbBr_3$ perovskite nanocrystals. Adv Opt Mater 6:1701106
9. Li Z, Hu Q, Tan Z, Yang Y, Leng M, Liu X, Ge C, Niu G, Tang J (2018) Aqueous synthesis of lead halide perovskite nanocrystals with high water stability and bright photoluminescence. ACS Appl Mater Interfaces 10:43915–43922

10. Carrizo AF, Belmonte GK, Santos FS, Backes CW, Strapasson GB, Schmidt LC, Rodembusch FS, Weibel DE (2021) Highly water-stable polymer–perovskite nanocomposites. ACS Appl Mater Interfaces 13:59252–59262
11. Zhuang W, Yao D, Li M, Xu W, Cen Q, Zhang M, Li H, Yan X, Zhang H (2024) Synergistically enhanced water-resistive perovskite nanocrystals for cell nucleus imaging and acid phosphatase detection. Sens Actuators B: Chem 416:136014
12. Lei Y, Bai L, Liang H, Cheng J, Xu Z, Li T, Chen S, Zhang D (2024) Enhanced thermal and water stability of halide perovskite $MAPbBr_3$ by double-coated hydrogen-bonded polymer network. Appl Surf Sci 670:160711
13. Wang Y, Varadi L, Trinchi A, Shen J, Zhu Y, Wei G (2018) Li C Spray-assisted coil–globule transition for scalable preparation of water-resistant CsPbBr 3@PMMA perovskite nanospheres with application in live cell imaging. Small 14:1803156
14. Chen J, Huang X, Xu Z, Chi Y (2022) Alcohol-stable perovskite nanocrystals and their in situ capsulation with polystyrene. ACS Appl Mater Interfaces 14:33703–33711
15. Ghinaiya NV, Park TJ, Kailasa SK (2023) Synthesis of bright blue fluorescence and water-dispersible cesium lead halide perovskite quantum dots for the selective detection of pendimethalin pesticide. J Photochem Photobiol A 444:114980
16. Pramanik A, Patibandla S, Gao Y, Gates K, Ray PC (2021) Water triggered synthesis of highly stable and biocompatible 1D nanowire, 2D nanoplatelet, and 3D nanocube $CsPbBr_3$ perovskites for multicolor two-photon cell imaging. JACS Au 1:53–65
17. Patel MR, Chetti P, Park TJ, Kailasa SK (2024) Fluorescence sensing of bilirubin using water-stable ethylenediaminetetraacetic acid-functionalized $CsPbBr_3$ perovskite quantum dots. ACS Appl Nano Mater 7:22640–22649
18. Ahlawat M, Neelakshi, Ramapanicker R, Rao VG (2023) Design principle of a water-dispersed photocatalytic perovskite through ligand deconstruction. ACS Energy Lett 8:2159–2168
19. Prochazkova AJ, Scharber MC, Yumusak C, Jančík J, Másilko J, Brüggemann O, Weiter M, Sariciftci NS, Krajcovic J, Salinas Y, Kovalenko A (2020) Synthesis conditions influencing formation of $MAPbBr_3$ perovskite nanoparticles prepared by the ligand-assisted precipitation method. Sci Rep 10:15720
20. Ju D, Lin G, Zhou M, Hua Y, Li X, Li H, Liu J (2022) Water-stable and hydrophobicity tunable organolead halide materials with Pb–N coordination for electrochemical CO_2 reduction. J Mater Chem A 10:17752–17759
21. Zheng L, Jiang K, Li X, Hong P, Chen K, Zhang H, Song Y, Luo B (2021) Water-assisted preparation of ethanol-dispersed $CsPbBr_3$ perovskite nanocrystals and emissive gel. J Colloid Interface Sci 598:166–171
22. Sun J, Li QF, Li X, Yan C, Wang G (2024) Super stable and water-dispersible $CsPbBr_3$ perovskite quantum dots for the efficient detection of Cu (II) and glutathione. Microchem J 199:110043
23. Liu JZ, Fu YB, Yang N, Wen QL, Li RS, Ling J, Cao Q (2024) Synthesis of a water-stable fluorescence $CsPbBr_3$ perovskite by dual-supersaturated recrystallization method and tuning the fluorescence spectrum for selective detection of folic acid. Spectrochim Acta A Mol Biomol Spectrosc 306:123586
24. Xu T, Xiahou J, Huang S, Liu Z, Li J (2024) Dispersion in water of $CsPbBr_3$ perovskite nanocrystals by surface modification. Ceram Int 50:15037–15043
25. Li Q, Xu K, Fan S, Zhang H, Wei X, Xu C, Luan X, Wang Z, Peng H, Shi L (2025) Aqueous phase synthesis of all-inorganic halide perovskite $CsPbCl_xBr_{3-}x$ nanocrystals using CsTFA as cesium source and surface ligand. Next Mater 6:100322
26. Chatterjee S, Khan T, Sen A, Das N, Sen P (2022) Massive amplification of photoluminescence and exceptional water stability of $MAPbBr_3$ nanocrystals through core–shell nanostructure formation in a self-defence mechanism. Mater Adv 3:7360–7369
27. Guo X, Lv Y, Wang L, Liu H, Wang W (2024) $CsPbBr_3$ perovskite quantum dots by mesoporous silica encapsulated for enhancing water and thermal stability via high temperature solid state method. Opt Mater 157:116097
28. Gunnarsson WB, Xu Z, Noel NK, Rand BP (2022) Improved charge balance in green perovskite light-emitting diodes with atomic-layer-deposited Al_2O_3. ACS Appl Mater Interfaces 14:34247–34252
29. Cuan J, Zhang D, Xing W, Han J, Zhou H, Zhou Y (2021) Confining $CsPbX_3$ perovskites in a hierarchically porous MOF as efficient and stable phosphors for white LED. Chem Eng J 425:131556
30. Mo Q, Chen C, Cai W, Zhao S, Yan D, Zang Z (2021) Room temperature synthesis of stable zirconia-coated $CsPbBr_3$ nanocrystals for white light-emitting diodes and visible light communication. Laser Photonics Rev 15:2100278
31. Li ZJ, Hofman E, Li J, Davis AH, Tung CH, Wu LZ, Zheng W (2017) Photoelectrochemically active and environmentally stable $CsPbBr_3/Ti_{O2}$ core/shell nanocrystals. Adv Funct Mater 28:1704288
32. Guptasarma P, Balasubramanian D, Matsugo S, Saito I (1992) Hydroxyl radical mediated damage to proteins, with special reference to the crystallins. Biochemistry 31:4296–4303
33. Cudina I, Jovanović SV (1988) Free radical inactivation of trypsin. Inter Radiat Phys Chem 32:497–501
34. Nosaka Y, Nosaka AY (2017) Generation and detection of reactive oxygen species in photocatalysis. Chem Rev 117:11302–11336
35. Cho H-Y, Mavi A, Sy-T D. Chueng, Pongkulapa T, Pasquale N, Rabie H, Han J, Kim JH, Kim T-H, Choi J-W, Lee K-B (2019) Tumor homing reactive oxygen species nanoparticle for enhanced cancer therapy. ACS Appl Mater Interfaces 11:23909–23918
36. Schafer FQ, Buettner GR (2001) Redox environment of the cell as viewed through the redox state of the glutathione disulfide/glutathione couple. Free Radical Biol Med 30:1191–1212
37. Tong L, Chuang CC, Wu S, Zuo L (2015) Reactive oxygen species in redox cancer therapy. Cancer Lett 367:18–25
38. Peterson KL, Margherio MJ, Doan P, Wilke KT, Pierre VC (2013) Basis for sensitive and selective time-delayed luminescence detection of hydroxyl radical by lanthanide complexes. Inorg Chem 52:9390–9398
39. Dickinson BC, Chang CJ (2011) Chemistry and biology of reactive oxygen species in signaling or stress responses. Nat Chem Biol 7:504–511
40. Xu Y, Ding J, Zhang C, Zhao M, Zhu S, Rao G, Zhang W, Zhang Z, Ma J (2023) A precise method to monitor hydroxyl radical in natural waters based on a fluoride-containing fluorescence probe. Sci Total Environ 903:166961
41. Shinde SS, Bhosale CH, Rajpure KY, Lee JH (2014) Remediation of wastewater: role of hydroxyl radicals. J Photochem Photobiol B 141:210–216
42. Khan ZUlH, Gul NS, Sabahat S, Sun J, Tahir K, Shah NS, Muhammad N, Rahim A, Imran M, Iqbal J, Khan TM, Khasim S, Farooq U, Wu J (2023) Removal of organic pollutants through hydroxyl radical-based advanced oxidation processes. Ecotoxicol Environ Saf 267:115564
43. Amor C, Fernandes JR, Lucas MS, Peres JA (2021) Hydroxyl and sulfate radical advanced oxidation processes: application to an agro-industrial wastewater. Environ Technol Innov 21:101183
44. Meng L, Wu Y, Yi T (2014) A ratiometric fluorescent probe for the detection of hydroxyl radicals in living cells. Chem Commun 50:4843–4845

45. Oka T, Yamashita S, Midorikawa M, Saiki S, Muroya Y, Kamibayashi M, Yamashita M, Anzai K, Katsumura Y (2011) Spin-trapping reactions of a novel gauchetype radical trapper G-CYPMPO. Anal Chem 83:9600–9604
46. Zhou W, Cao Y, Sui D, Lu C (2016) Turn-on luminescent probes for the real-time monitoring of endogenous hydroxyl radicals in living cells. Angew Chem 128:4308–4313
47. Ganea GM, Kolic PE, El-Zahab B, Warner IM (2011) Ratiometric coumarin–neutral red (CONER) nanoprobe for detection of hydroxyl radicals. Anal Chem 83:2576–2581
48. Zhu B-Z, Mao L, Huang C-H, Qin H, Fan R-M, Kalyanaraman B, Zhu J-G (2012) Unprecedented hydroxyl radical-dependent two-step chemiluminescence production by polyhalogenated quinoid carcinogens and H_2O_2. Proc Natl Acad Sci U S A 109:16046
49. Xue Y, Luan Q, Yang D, Yao X, Zhou K (2011) Direct evidence for hydroxyl radical scavenging activity of cerium oxide nanoparticles. J Phys Chem C 115:4433–4438
50. Joshi DJ, Jha S, Malek NI, Park TJ, Kailasa SK (2024) Rational design of niobium carbide MXene quantum dots decorated with arginine for the fluorescence sensing of superoxide anion in Saccharomyces cerevisiae cells. Sens Actuators B-Chem 404:135226
51. Janik I, Bartels DM, Jonah CD (2007) Hydroxyl radical self-recombination reaction and absorption spectrum in water up to 350 °C. J Phys Chem A 111:1835–1843
52. Linxiang L, Abe Y, Nagasawa Y, Kudo R, Usui N, Imai K, Mashino T, Mochizuki M, Miyata N (2004) An HPLC assay of hydroxyl radicals by the hydroxylation reaction of terephthalic acid. Biomed Chromatogr 18:470–474
53. Harshita TJ, Park SK (2023) Kailasa, Microwave-assisted synthesis of green fluorescent copper nanoclusters: a novel approach for sensing of hydroxyl radicals and pyrophosphate ions via a "turn-off–on" mechanism. New J Chem 47:20038–20047
54. Sadhu VA, Jha S, Park TJ, Kailasa SK (2024) Green emissive molybdenum nanoclusters for selective and sensitive detection of hydroxyl radical in water samples. J Fluoresc. https://doi.org/10.1007/s10895-023-03578-5
55. Wu S, Ma C, Gao Y, Su Y, Xia Q, Chen Z, Zhu J-J (2020) Dynamic detection of endogenous hydroxyl radicals at single-cell level with individual Ag–Au nanocages. Anal Chem 92:9940–9947
56. Bhattacharya S, Sarkar R, Nandi S, Porgador A, Jelinek R (2017) Detection of reactive oxygen species by a carbon-dot–ascorbic acid hydrogel. Anal Chem 89:830–836
57. Wu Y, Huang W, Peng D, Huang X, Gu J, Wu S, Deng T, Liu F (2021) Synthesis of dihydroquinolines as scaffolds for fluorescence sensing of hydroxyl radical. Org Lett 23:135–139
58. Qin F, Padhiar MA, Pan S, Khan NZ, Ji Y, Khan SA, Ahmed J, Zhang S (2024) Mn^{2+}-doped $CsPbCl_3$ nanocrystals for ammonia gas sensing. ACS Appl Nano Mater 7:10614–10624
59. Yang L, Cui Y, Hu B, Yang Q, Xu X (2024) Highly luminescent and water-stable $CsPbCl_3/Mn^{2+}$/PEG nanocrystals for ultrasensitive detection of 4-nitrophenol. ACS Appl Nano Mater 7:5146–5155
60. Gong M, Sakidja R, Goul R, Ewing D, Casper M, Stramel A, Elliot A, Wu JZ (2019) High-performance all-inorganic $CsPbCl_3$ perovskite nanocrystal photodetectors with superior stability. ACS Nano 13:1772–1783
61. Zhao Z, Xu W, Pan G, Liu Y, Yang M, Hua S, Chen X, Peng H, Song H (2019) Enhancing the exciton emission of $CsPbCl_3$ perovskite quantum dots by incorporation of Rb^+ ions. Mater Res Bull 112:142–146
62. Yu H, Gao X, Huang C, Liu S, Chen B, Xu S, Zhang Y, Zhao H (2023) $CsPbCl_3$ and Mn:$CsPbCl_3$ perovskite nanocubes/nanorods as a prospective cathode material for LIB application. J Mater Sci Mater Electron 34:1582
63. Liu S, Zhao J, Zhang K, Yang L, Sun M, Yu H, Yan Y, Zhang Y, Wu L, Wang S (2016) Dual-emissive fluorescence measurements of hydroxyl radicals using a coumarin-activated silica nanohybrid probe. Analyst 141:2296–2302
64. Jia Q, Liu Y, Duan Y, Zhou J (2019) Interference-free detection of hydroxyl radical and arthritis diagnosis by rare earth-based nanoprobe utilizing SWIR emission as reference. Anal Chem 91:11433–11439
65. Garima S, Jindal S, Garg I, Matai G, Packirisamy A (2021) Sachdev, Dual-emission copper nanoclusters–based ratiometric fluorescent probe for intracellular detection of hydroxyl and superoxide anion species. Microchim Acta 188:13
66. Chai Y, Gao Z, Li Z, He L, Yu F, Yu S, Wang J, Tian Y, Liu L, Wang Y, Wu Y (2020) A novel fluorescent nanoprobe that based on poly(thymine) single strand DNA-templated copper nanocluster for the detection of hydrogen peroxide. Spectrochim Acta A Mol Biomol Spectrosc 239:118546
67. Sun M, Su Y, Yang W, Zhang L, Hu J, Lv Y (2019) Organosiloxane and polyhedral oligomeric silsesquioxanes compounds as chemiluminescent molecular probes for direct monitoring hydroxyl radicals. Anal Chem 91:8926–8932
68. Huang Z, Ji Z, Yin P, Shu Y, Xu Q, Hu XY (2019) Salicylic acid impregnated activated carbon fiber paper: an effective platform for the simple and sensitive detection of hydroxyl radicals in the atmosphere. Electrochem Commun 100:113–116
69. Zhuang M, Ding C, Zhu A, Tian Y (2014) Ratiometric fluorescence probe for monitoring hydroxyl radical in live cells based on gold nanoclusters. Anal Chem 86(3):1829–1836
70. Xie Y, Xianyu Y, Wang N, Yan Z, Liu Y, Zhu K, Hatzakis NS (2018) X Jiang Functionalized gold nanoclusters identify highly reactive oxygen species in living organisms. Adv Funct Mater 28:1702026